

An Optimally Controlled Variable Output Wound Rotor Synchronous Machine

James O. Owuor¹, Josiah L. Munda², and Adisa A. Jimoh²

¹Electrical Department, Masinde Muliro University of Science & Technology, Kakamega, Kenya

²Department of Electrical Engineering, Tshwane University of Technology, Pretoria, South Africa

Email: jowuor@mmust.ac.ke, {mundajl, jimohaa}@tut.ac.za

Abstract—This paper presents analytical and simulation results for a wound rotor synchronous machine in variable speed, variable output applications. To enable efficient control, an optimized LQR strategy is employed. For secure power supply to the loads, the machine only operates in the generating mode. The concept presented provides great flexibility in operation of the synchronous machine and is suitable for small hydropower and wind generation applications. The method enhances efficiency in the control of synchronous generators.

Index Terms—variable speed, synchronous machine, optimal control, linear quadratic regulator

I. INTRODUCTION

Machine configurations for different applications broadly fall into either the fixed or adjustable speed category, most of which are employed in wind and hydropower generation, electric vehicles and marine propulsion among others [1]-[6].

In general, variable speed configurations offer greater flexibility and adaptability. In variable speed applications, a major drawback with the DFIG is that it needs a source of excitation. Common problems with Variable Speed Drives (VSD) employing DFIGs in general, are related to drops in the dc voltage link level either due to the inability of the grid side converter to supply adequate power to the dc bus during a load side system fault, or total absence of a stable source of power in the case of an isolated power system, especially during sustained events. The synchronous machine responds well in such cases because of its independent excitation system.

The permanent magnet synchronous machine is more efficient than its electrically excited counterpart, eliminates copper losses, and is also generally smaller in size, but its magnetic characteristics change with time [7]. In addition, there are limits to the control of the air-gap flux levels since there is no control of excitation.

The proposed scheme offers the following advantages:

- Distribution network stability can be improved in areas with weak grid coupling.
- The plant can work in an autonomous way; the synchronous machine always provides a way of charging the converter dc link without the need of an auxiliary source.

- May allow increased percentage penetration of other renewable energy generation e.g. solar and wind into distribution networks.
- Provides a responsive and efficient means of quickly ramping generation up or down when load demands.

This paper models the steady state and dynamic behaviour of the proposed scheme using Matlab/Simulink and compares two methods of generating reference currents for controlling the generator loading and D.C. bus power balance.

II. SYSTEM DESCRIPTION

The proposed scheme comprises of a Synchronous Machine (SM) connected to an uncontrolled load commutated diode rectifier connected to the synchronous machine stator. Output to the system is via a PWM bi-directional vector controlled inverter. A capacitor connected in the DC link decouples operation of the two converters and a Battery Energy Storage System (BESS) with a bidirectional DC-DC converter is also connected in the DC link. This arrangement is such that the synchronous machine takes care of the slower electro-dynamics while a DC-DC converter and BESS take care of the faster electro-dynamics associated with the system. The machine speed is allowed to vary within a limited range that is bounded by its synchronising torque limits.

III. MODELLING AND SIMULATION SYSTEM DESIGN OVERVIEW

Steady state defined plant operational modes are determined by an external power set-point P_{set} which sets the system power balance mode. This set point is used as the main input to the control system and can be set based on scheduled operation. Since the set-point rate of update is relatively slow, the main scope of interest here is the response of the system to power fluctuations.

TABLE I. SYSTEM OPERATION MODES

Power Balance Mode	System Speed
$P_{set} - P_l > P_l^{max} + P_1$	$> \omega_{syn}$
$P_{set} - P_l = P_l^{max} + P_1$	$= \omega_{syn}$
$P_{set} - P_l < P_l^{max} + P_1$	$< \omega_{syn}$

Table I gives a summary of defined operational modes. In the table, P_{set} is the external power set-point, P_l is the actual local load, P_l^{max} is the maximum local load, and P_i is the inverter output power.

IV. INPUT OUTPUT POWER RELATIONS

Fig. 1 shows the power relations in the proposed system. These derived relations between input and output powers assume negligible rotor and stator resistances, leakage inductances and friction and windage losses.

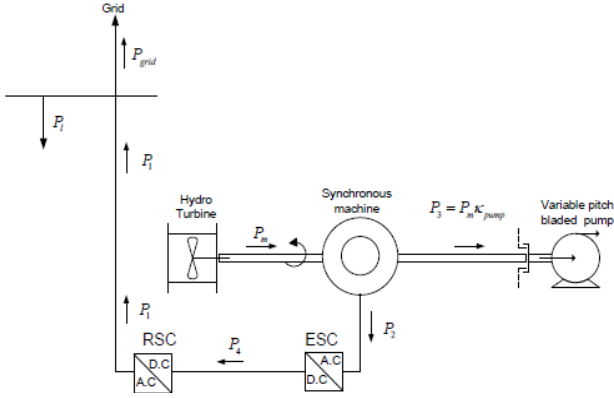


Figure 1. System power relations.

$P_1 = V_1 I_1 \cos \phi_1$ is the inverter output power and P_2 is the synchronous machine electrical power output, supplying a diode rectifier load. The magnitude of this load is determined by the dc link voltage level [8]. The model used here represents the fundamental harmonic components of the machine ac variables and the average value of the dc variables, while accounting for the effects of the non-ideal diodes.

In order to quantify the output power of the synchronous machine, it is necessary to express the generator equivalent inductance as an equivalent subtransient commutating inductance because of the diode rectifier at its terminals [9]. Neglecting resistances, equivalent circuits of d- and q-axis subtransient inductances are obtained with standard notations, where L_{aq} and L_{ad} are the magnetising and the stator leakage inductances, $L_{kq\sigma}$, $L_{kd\sigma}$ are the q- and d-axis leakage inductances and $x_{fd\sigma}$ is the field winding leakage inductance. The equivalent inductance L_t'' is used to express the generator reactance because the switching actions of the diodes are much faster than the generator's dynamics.

Assuming no change in load current within one switching period, the transient commutating inductance for a synchronous machine connected to a converter is defined as:

$$L_t(\beta) = L_d'' + L_q'' + (L_d'' - L_q'') \sin\left(2\beta - \frac{\pi}{6}\right) \quad (1)$$

For a diode rectifier, $\beta = 0$. Given that closed-loop subtransient impedance is almost equal to open-loop subtransient impedance, the open-loop subtransient

impedance can be used to represent generator behaviour and (2) gives the commutating reactance.

$$L_t'' = 0.5L_d'' + 1.5L_q'' \quad (2)$$

The synchronous machine power, P_2 , may then be quantified thus:

$$P_2 = \frac{\left(\frac{E_{af}}{\omega_e}\right) V_t}{2L_t''} \sin(2\delta) \quad (3)$$

Equation (3) differs from the familiar steady state power-torque angle equation in the $\sin(2\delta)$ term. The transient power-torque angle curve is in other words, a function of $\sin(2\delta)$ [10]. This has an important implication for the steady state stability limit of the synchronous machine, and hence stability of its power output. The critical torque angle for such a machine is given by:

$$\delta_{cr} = \sin^{-1} \frac{P_2 L_t''}{\left(\frac{E_{af}}{\omega_e}\right) V_t} \quad (4)$$

The dependence of P_2 on speed and excitation voltage E_{af} is seen in (3). E_{af} can be regulated with changes in speed by appropriate field excitation. As noted earlier, the load seen by the synchronous machine is determined by the dc link voltage level and in order to ensure proper energy balance in the system, this voltage, and by extension V_t of (3) needs to be managed. This means that there must be supplementary means of balancing demand-generation mismatches in the dc bus. This is accomplished by the Battery Energy Storage System (BESS) and dc-dc converter.

The dc link power P_4 is given by:

$$P_4 = v_{dc} i_{dc} \quad (5)$$

V. SYSTEM MODEL

A. Synchronous Machine Model

The synchronous machine model used here is derived from [10] in the rotor reference dq-frame with currents as state variables.

B. ESC Converter Model

The average values of synchronous machine fundamental harmonic d-q variables are directly related to the dc voltage and current at the diode output. The model is an adaptation from [11], [12] and includes components during the commutation and conduction periods. The equations are averaged within one switching period as shown in (6).

$$\hat{v}_{dc} = \frac{3\sqrt{3}}{\pi} V - \frac{3\omega L_c}{\pi} I_d - 2L_c \frac{di_{dc}}{dt} \quad (6)$$

The expressions for the average stator ac currents in the d-q frames respectively are:

$$\hat{i}_{qs} = \frac{3}{\pi} \left(\int_{\pi/3}^{\pi/3+\mu} i_{q,com}(t) \cdot dt + \int_{\pi/3+\mu}^{2\pi/3} i_{q,con}(t) \cdot dt \right) \quad (7)$$

$$\begin{aligned} &= \hat{i}_{q,com} + \hat{i}_{q,con} \\ \hat{i}_{ds} &= \frac{3}{\pi} \left(\int_{\pi/3}^{\pi/3+\mu} i_{d,com}(t) \cdot dt + \int_{\pi/3+\mu}^{2\pi/3} i_{d,con}(t) \cdot dt \right) \quad (8) \\ &= \hat{i}_{d,com} + \hat{i}_{d,con} \end{aligned}$$

where $\hat{i}_{q,com}$, $\hat{i}_{d,com}$ are q-d input currents in the commutation period, $\hat{i}_{q,con}$, $\hat{i}_{d,con}$ are q-d input currents in the conduction period, and μ is the commutation angle.

The power P_2 input to the diode rectifier is quantified as:

$$P_{2,in} = v_{ds}^r \hat{i}_{ds}^r + v_{qs}^r \hat{i}_{qs}^r = \hat{v}_{dc} \hat{i}_{dc} \quad (9)$$

C. RSC Converter Model

The RSC voltage equations in the d-q grid voltage synchronous reference frame are given as follows:

$$\hat{v}_{qg}^s = \hat{d}_{q1} \hat{v}_{dc} + \omega_s L_g \hat{i}_{qg}^s - L_g \frac{d\hat{i}_{dg}^s}{dt} \quad (10)$$

$$\hat{v}_{dg}^s = \hat{d}_{d1} \hat{v}_{dc} - \omega_s L_g \hat{i}_{dg}^s - L_g \frac{d\hat{i}_{qg}^s}{dt} \quad (11)$$

$$\hat{v}_{dc}^s = -\left[\hat{d}_{qd1}^T \cdot R_g \hat{i}_{qdg}^s \right] - R_g C \frac{dV_{dc}}{dt} \quad (12)$$

ω_s is the grid side angular frequency and the superscript

s refers to the reference frame. Also, $\hat{i}_{qdg}^s = \left[\hat{i}_{qg}^s, \hat{i}_{dg}^s \right]^T$ and $\hat{d}_{qd1}^s = \left[\hat{d}_{q1}^s, \hat{d}_{d1}^s \right]$ and elements with subscript 'g' are load side or grid quantities.

D. Battery Energy Storage System (BESS) Converter and D.C. Link Models

The BESS converter balances demand-generation mismatches in the dc bus by supporting the dc bus voltage. Neglecting switching, converter and dc bus losses, the converter dynamics are expressed in (13).

$$v_{batt} = L_{batt} \frac{di_{batt}}{dt} + v_{dc} (1 - d_{batt}) \quad (13)$$

where d_{batt} is the converter duty cycle.

The dynamics combining the dc link capacitor and battery are governed by (14).

$$\begin{aligned} C \frac{dv_{dc}}{dt} &= i_{batt} (1 - d_{batt}) - i_{RSC} - i_{ESC} \\ &= i_c = i_{dc} - i_{RSC} - i_{ESC} \end{aligned} \quad (14)$$

As can be deduced from (14), during steady state operation, the governing power balance in the dc link is given by (15).

$$P_{batt} = P_{ESC} + P_{RSC} \quad (15)$$

And the dc current is given by:

$$i_{dc} = i_{ESC} + i_{RSC} \quad (16)$$

Under steady state conditions, it is therefore maintained at constant value. In case of a disturbance, a mismatch occurs in the power balance of (15), causing currents of (14) to flow through the capacitor. The battery in this case either charges or discharges, to absorb or supply the appropriate amount of current to maintain v_{dc} .

E. Battery Energy Storage System (BESS) Model

The battery is modelled using a controlled voltage source in series with a constant resistance [13]. The charge and discharge cycles are assumed to have the same characteristics.

VI. CONTROL STRATEGY

A. Optimal Control of Synchronous Machine and DC-DC Converter

From (3), a degree of freedom is provided by the $\left(\frac{E_{af}}{\omega_e} \right)$ ratio. Under these conditions, the generator power (load) can be controlled through control of the DC link current I_L through the dc-dc booster while the field current I_f controls $\left(\frac{E_{af}}{\omega_e} \right)$. Because of the nature of the configuration, it is convenient to divide the operation of the synchronous generator into two control areas as seen in Fig. 2. The shaded area bounded by $0.7\omega_s \geq \omega_s \leq 1.3\omega_s$ defines the speed variation limits.

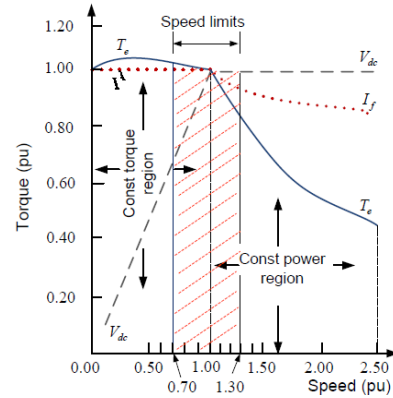


Figure 2. Operating regions.

An optimal control strategy [14], [15] with a Linear Quadratic Regulator (LQR) [16] incorporating integral control action presents an attractive strategy for controlling the synchronous machine and dc-dc converter. The state equation of the plant is linear, the cost function is quadratic and the control method covers the shaded operating range of Fig. 2.

The proposed synchronous machine optimal control structure is a modified Field Oriented Control (FOC) and is shown in Fig. 3 with $T_{e,ext}^*$ as the external system torque

command. The optimal reference current block simultaneously provides stator and excitation current references which are generated off-line. The PWM block outputs the duty cycle commands d_q, d_d while the exciter duty cycle modulator outputs its power stage duty cycle commands.

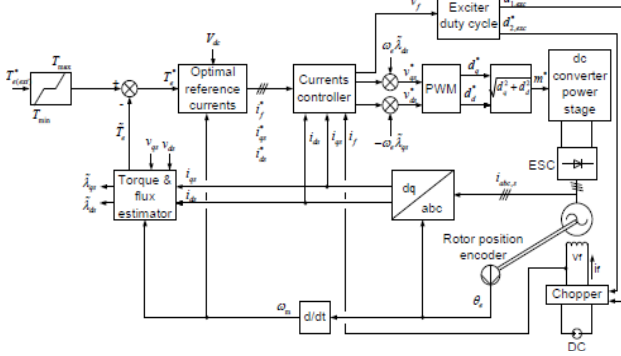


Figure 3. Optimal control structure.

The state variable coefficient matrices $\mathbf{A}_1, \mathbf{B}_1, \mathbf{C}_1$ with unsaturated parameters [10] are given below:

$$\mathbf{A}_1 = \begin{bmatrix} \frac{R_s L_f}{D_1} & -\frac{\omega_e L_f L_{qs}}{D_1} & -\frac{R_f L_{md}}{D_1} \\ -\frac{\omega_e L_{ds}}{L_{qs}} & -\frac{R_s}{L_{qs}} & -\frac{\omega_e L_{md}}{L_{qs}} \\ -\frac{R_s L_{md}}{D_1} & -\frac{\omega_e L_{md} L_{qs}}{D_1} & -\frac{R_f L_{ds}}{D_1} \end{bmatrix} \quad (17)$$

$$\mathbf{B}_1 = \begin{bmatrix} \frac{L_f}{D_1} & 0 & -\frac{L_{md}}{D_1} \\ 0 & -\frac{1}{L_{qs}} & 0 \\ -\frac{L_{md}}{D_1} & 0 & -\frac{L_{ds}}{D_1} \end{bmatrix} \quad (18)$$

$$\mathbf{C}_1 = \begin{bmatrix} 0 & 0 & 0 \\ 0 & 0 & 0 \\ 0 & 0 & 1 \end{bmatrix} \quad (19)$$

where $D_1 = L_f L_{ds} - L_{md}^2$ and speed is seen as an external parameter imposed by the prime mover.

Equations (17), (18) and (19) lead to the state space form:

$$\begin{aligned} \dot{x} &= \mathbf{A}x + \mathbf{B}u \\ y &= \mathbf{C}x \end{aligned} \quad (20)$$

with $x = [i_{qs}^r, i_{ds}^r, i_{fd}^r]^T$ as the state vector, $u = [0, 0, v_{fd}^r]^T$ as the input vector, and $y = [i_{qs}^r, i_{ds}^r, i_{fd}^r]^T$ as the output vector. The synchronous machine portion of the combined machine/rectifier equations considered here only has one degree of freedom in the input v_{fd}^r .

The dc-dc converter is assumed to operate in continuous conduction mode. Neglecting harmonics in

the average power delivered (equivalent to considering only the DC component of the switching function), the state variable model of the dc side is given by:

$$\frac{d\hat{V}_{dc}}{dt} = \frac{\hat{v}_{ds} \hat{i}_{ds} + \hat{v}_{qs} \hat{i}_{qs}}{C\hat{V}_{dc}} - \frac{i_L}{C} \quad (21)$$

$$\frac{di_L}{dt} = -\frac{R_L}{L_L} i_L + \frac{V_{dc}}{L_L} \quad (22)$$

The switching functions d_d, d_q and dc voltage V_{dc} are related to the rectifier input voltages v_{qs} and v_{ds} through the following expressions:

$$\sqrt{2}v_{ds} = d_d V_{dc}; \quad \sqrt{2}v_{qs} = d_q V_{dc} \quad (23)$$

The modulation index m and phase angle ϕ are used to control the dc-dc converter and their relations with d_q, d_d and δ delta are:

$$m = \sqrt{d_q^2 + d_d^2}; \quad \phi = \omega_t + \delta \quad (24)$$

and $\delta = \tan^{-1}(d_q / d_d)$.

After linearising (20), (21), (22) and substituting (23) into (21), (22), the affine equations are:

$$\begin{aligned} \dot{x}(t) &= \mathbf{A}_v x(t) + \mathbf{B}_v u(t) \\ y(t) &= \mathbf{C}_v x(t) \end{aligned} \quad (25)$$

where $x(t) = [i_{qs}^r, i_{ds}^r, i_{fd}^r, V_{dc}, i_L]^T$, $u(t) = [v_{fd}^r, d_q, d_d]^T$ and:

$$\mathbf{A}_v = \begin{bmatrix} \frac{R_s L_f}{D_1} & -\frac{\omega_e L_f L_{qs}}{D_1} & -\frac{R_f L_{md} d_{qs0}}{D_1} & 0 & 0 \\ -\frac{\omega_e L_{ds}}{L_{qs}} & -\frac{R_s}{L_{qs}} & -\frac{\omega_e L_{md} d_{ds0}}{L_{qs}} & 0 & 0 \\ -\frac{R_s L_{md}}{D_1} & -\frac{\omega_e L_{md} L_{qs}}{D_1} & -\frac{R_f L_{ds}}{D_1} & 0 & 0 \\ \frac{d_{qs0}}{\sqrt{2}C} & \frac{d_{ds0}}{\sqrt{2}C} & 0 & 0 & -\frac{1}{C} \\ 0 & 0 & 0 & \frac{1}{L_L} & -\frac{R_L}{L_L} \end{bmatrix} \quad (26)$$

$$\mathbf{B}_v = \begin{bmatrix} \frac{V_{dc0} L_f}{\sqrt{2}D_1} & 0 & -\frac{L_{md}}{D_1} \\ \frac{V_{dc0} L_{md}}{\sqrt{2}D_1} & 0 & \frac{L_{ds}}{D_1} \\ \frac{i_{qs0}}{\sqrt{2}C} & \frac{i_{ds0}}{\sqrt{2}C} & 0 \end{bmatrix} \quad (27)$$

The output vector is $y = \mathbf{C}_v x(t) = [i_{ds}^r, i_{fd}^r, V_{dc}]^T$, where:

$$\mathbf{C}_v = \begin{bmatrix} 0 & 1 & 0 & 0 & 0 \\ 0 & 0 & 1 & 0 & 0 \\ 0 & 0 & 0 & 1 & 0 \end{bmatrix} \quad (28)$$

B. Optimal Control Strategy with Integral Action

Integral action is provided by adding an extra set of variables into the small signal model of (25) [16] and the augmented state model is:

$$\begin{aligned}\dot{\mathbf{z}}(t) &= \mathbf{A}_0 \mathbf{z}(t) + \mathbf{B}_0 \mathbf{u}(t) \\ \mathbf{y}(t) &= \mathbf{C}_0 \mathbf{z}(t)\end{aligned}\quad (29)$$

where $\mathbf{z}(t) = [i_{qs}^r, i_{ds}^r, i_{fd}^r, V_{dc}, i_L, \int i_{ds}^r, \int i_{fd}^r, \int V_{dc}]^T$ is the augmented state vector. The new \mathbf{A}_0 , \mathbf{B}_0 , \mathbf{C}_0 matrices are:

$$\mathbf{A}_0 = \begin{bmatrix} \mathbf{A}_v & \mathbf{O}_{5,3} \\ \mathbf{C}_v & \mathbf{O}_3 \end{bmatrix}; \quad \mathbf{B}_0 = \begin{bmatrix} \mathbf{B}_v \\ \mathbf{O}_3 \end{bmatrix}; \quad \mathbf{C}_0 = [\mathbf{C}_v \quad \mathbf{O}_3] \quad (30)$$

and $\mathbf{O}_{5,3}$ is a 5×3 zero matrix, while \mathbf{O}_3 is a 3×3 matrix.

The discrete form of (29) is:

$$\begin{aligned}\mathbf{z}(k+1) &= \Phi \mathbf{z}(k) + \Gamma \mathbf{u}(k) \\ \mathbf{y}(k) &= \mathbf{C}_0 \mathbf{z}(k)\end{aligned}\quad (31)$$

where $\Phi = e^{\mathbf{A}_0 T_s}$, $\Gamma = \int_0^{T_s} e^{\mathbf{A}_0 \tau} d\tau$ and T_s is the sampling

time. For infinite horizon LQR, the following cost function is minimised with the pre-conditions: controllability of $(\mathbf{A}_0, \mathbf{B}_0)$, and observability of $(\mathbf{C}_0, \mathbf{A}_0)$.

$$J(\mathbf{z}(k), \mathbf{u}(k)) = \sum_{k=0}^{\infty} [\mathbf{z}^T(k) \mathbf{Q} \mathbf{z}(k) + \mathbf{u}^T(k) \mathbf{R} \mathbf{u}(k)] \quad (32)$$

\mathbf{Q} and \mathbf{R} are weighting diagonally symmetric positive definite matrices that penalize the state and control effort respectively. The problem is to find a gain matrix \mathbf{K}_c such that the control function of \mathbf{u} minimises (32).

The matrix gain is expressed as:

$$\mathbf{K}_c = -\mathbf{R}^{-1} \mathbf{B}^T \mathbf{P}_c \quad (33)$$

where \mathbf{P}_c is the solution to the following Discrete Algebraic Riccati Equation (DARE) [17]:

$$\mathbf{P}_c \Phi + \Phi^T \mathbf{P}_c - \mathbf{P}_c \Gamma \mathbf{R}^{-1} \mathbf{B}^T \mathbf{P}_c + \mathbf{Q} = 0 \quad (34)$$

The control is optimized among all the integrable signals $\mathbf{u}_c(t)$ and the resulting optimal control law is given by:

$$\mathbf{u}_c(k) = -\mathbf{K}_c \mathbf{z}(k) \quad (35)$$

Once the weighting matrices \mathbf{Q} and \mathbf{R} are chosen, the cost function to be minimised is expressed as follows:

$$\begin{aligned}J(\mathbf{z}(k), \mathbf{u}(k)) &= \sum_{k=0}^{\infty} \left[Q_{i_{qr}^r} \cdot (i_{qr}^r)^2 + Q_{i_{dr}^r} \cdot (i_{dr}^r)^2 + Q_{i_{fd}^r} \cdot (i_{fd}^r)^2 \right. \\ &+ Q_{v_{dc}} \cdot (v_{dc})^2 + Q_{i_L} \cdot (i_L)^2 + Q_{i_{qs}^r} \cdot \{i_{qs}^{r*} - i_{qs}^r\}^2 \\ &+ Q_{i_{ds}^r} \cdot \{i_{ds}^{r*} - i_{ds}^r\}^2 + Q_{i_{fd}^r} \cdot \{i_{fd}^{r*} - i_{fd}^r\}^2 \\ &\left. + Q_{V_{dc}} \cdot \{V_{dc}^* - V_{dc}\}^2 + \mathbf{u}^T \mathbf{R} \mathbf{u} \right] \quad (36)\end{aligned}$$

where \mathbf{Q} is given as:

$$\mathbf{Q} = \begin{bmatrix} Q_{i_{qr}^r} & 0 & 0 & 0 & 0 & 0 & 0 & 0 & 0 \\ 0 & Q_{i_{dr}^r} & 0 & 0 & 0 & 0 & 0 & 0 & 0 \\ 0 & 0 & Q_{i_{fd}^r} & 0 & 0 & 0 & 0 & 0 & 0 \\ 0 & 0 & 0 & Q_{v_{dc}} & 0 & 0 & 0 & 0 & 0 \\ 0 & 0 & 0 & 0 & Q_{i_L} & 0 & 0 & 0 & 0 \\ 0 & 0 & 0 & 0 & 0 & Q_{i_{qs}^r} & 0 & 0 & 0 \\ 0 & 0 & 0 & 0 & 0 & 0 & Q_{i_{ds}^r} & 0 & 0 \\ 0 & 0 & 0 & 0 & 0 & 0 & 0 & Q_{i_{fd}^r} & 0 \\ 0 & 0 & 0 & 0 & 0 & 0 & 0 & 0 & Q_{V_{dc}} \end{bmatrix} \quad (37)$$

and \mathbf{R} is an \mathbf{I}_3 identity matrix.

C. Reference Currents

Assuming V_{dc}^* is provided, it is necessary to generate the optimal reference currents $i_{qs}^{r*}, i_{ds}^{r*}, i_{fd}^{r*}$ of (36). The synchronous machine operates in either of the two operating regions of Fig. 2. Operation in the constant torque region is generally implemented using Maximum Torque per Ampere (MTPA) mode while that in the constant power region is implemented in partial Field Weakening (FW) mode. Because of the three degrees of freedom, values of reference currents have to be calculated for each torque and speed duplex which points to a constrained optimisation problem.

Optimal reference currents $i_{qs}^{r*}, i_{ds}^{r*}, i_{fd}^{r*}$ are generated to maximize the efficiency in the whole torque-speed plane [18]. These currents can either be generated; off-line and stored in look-up tables, or on-the-fly as by demand, for the same control structure of Fig. 3. Both strategies are non-linear constrained optimisation problems. For simplicity, parameters are assumed not to vary. Formulation of the two strategies follows.

D. Optimal Reference Currents through Look-up

For this strategy, the problem is formulated as:

$$\begin{aligned}\forall (T^*, \Omega), \text{ minimise } & \sum P_l \\ & \text{s.t. } T_m = T^* \\ & v_{r.m.s} \leq v_{r.m.s}(\max) \\ & i_{r.m.s} \leq i_{r.m.s}(\max) \\ & i_{fd} \leq i_{fd}(\max)\end{aligned}\quad (38)$$

where P_l represents total losses (only C_u losses are considered here), T_m is mechanical input torque, $v_{r.m.s}(\max)$ is the maximum phase voltage, $i_{r.m.s}(\max)$ and $i_{fd}(\max)$ are stator and field current limits. For each operating point the following relations apply:

$$\begin{aligned}
 P_{cu} &= 3R_s i_{r.m.s}^2 + R_f i_{fd}^2 \\
 i_{r.m.s} &= \sqrt{(i_{ds}^r)^2 + (i_{qs}^r)^2} \\
 v_{r.m.s} &= \sqrt{(v_{ds}^r)^2 + (v_{qs}^r)^2} \\
 v_{qs}^r &= R_s i_{qs}^r + \omega_s \lambda_{ds}^r \\
 v_{ds}^r &= R_s i_{ds}^r - \omega_s \lambda_{qs}^r
 \end{aligned} \quad (39)$$

And from [10]:

$$T_e = L_{md} i_f i_{qs}^r + (L_d - L_q) i_{qs}^r i_{ds}^r \quad (40)$$

The constraints were formulated in terms of the following constraint functions g_t , g_i , g_v , and g_f , for torque, current and voltages respectively.

$$\begin{aligned}
 g_t &= |T_m - T^*| - \varepsilon |T^*| \\
 g_i &= i_{r.m.s} - i_{r.m.s,(max)} \\
 g_v &= v_{r.m.s} - v_{r.m.s,(max)} \\
 g_f &= v_{fd} - v_{fd,(max)}
 \end{aligned} \quad (41)$$

Using the Matlab optimiser f_{mincon} , an algorithm was developed to generate torque-speed maps for the entire torque-speed characteristics of the generator. This gave optimal values of i_{qs}^{r*} , i_{ds}^{r*} , i_{fd}^{r*} for each torque-speed duo. To minimise memory storage, the values stored in the simulation look-up table were limited to those within the operating speed $0.7\omega_s \leq \omega_s \leq 1.3\omega_s$.

E. Optimal Reference Currents Generated in Real Time

In this method, the optimal i_{qs}^{r*} , i_{ds}^{r*} , i_{fd}^{r*} currents are generated during simulation in real time through derived analytical expressions.

Below rated speed there are no voltage limitations, the machine is controlled in the constant torque region using the Maximum Torque per Ampere (MTPA) strategy. The torque per ampere ratio is maximised using the current vector. Above rated speed, it is controlled in the maximum power region using a flux weakening strategy [19], which is accomplished by reducing the d- axis component of the current. Both regions are illustrated in Fig. 2.

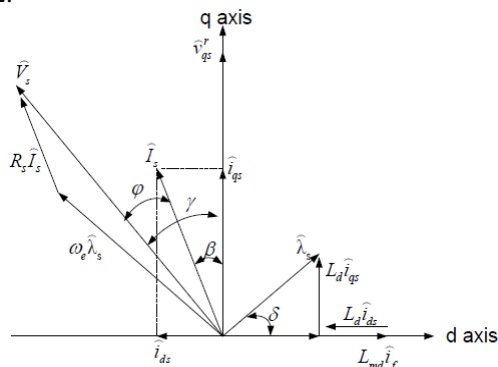


Figure 4. Synchronous machine phasor diagram.

The steady-state phasor diagram of Fig. 4 is obtained from machine equations in [10]. In the phasor diagram, the angles by which the stator current and voltage lead the q- axis, respectively, are denoted by β and γ , while δ is the torque angle. From the figure, the d-q stator currents are:

$$i_d = -\hat{I}_s \sin \beta; \quad i_q = \hat{I}_s \cos \beta \quad (42)$$

where I_s is the stator current amplitude. The torque expression of (43) in terms of the stator current amplitude is obtained by substituting (42) into (40).

$$T_e = -L_{md} i_f I_s \cos \beta + \frac{1}{2} I_s^2 (L_d - L_q) \sin(2\beta) \quad (43)$$

For MTPA, the relationship between I_s and β for maximum torque is derived by differentiating (43) with respect to β and equating the result to zero. Solving the differential for i_d gives the d- axis reference current as:

$$i_{ds}^* = \frac{L_{md} i_f^*}{(L_d - L_q)} - \sqrt{\frac{(L_{md} i_f^*)^2}{2(L_d - L_q)^2} - i_{qs}^{*2}} \quad (44)$$

From (44), MTPA is obtained if i_{ds}^* is determined for any i_{qs}^* and i_{fd}^* . The strategy involves switching between MTPA and flux weakening modes depending on the speed and torque status and is illustrated in Fig. 5 for the case of an interior permanent magnet machine [20].

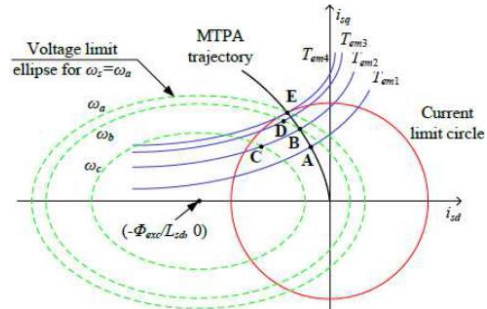


Figure 5. Torque trajectories.

In the figure, when the rotor electrical speed increases from ω_b to ω_c at constant torque, T_{em2} cannot be produced using the MTPA laws, therefore the operating point slides from B to C along the constant torque curve. Conversely, upon reaching the voltage limit for a given speed (see point B), the MTPA current laws cannot be applied. Attaining operating point D when $\omega_s = \omega_c$ requires sliding from point B along the voltage limit ellipse while the highest achievable torque for speeds equal to or below ω_s is T_{em4} . In this paper, the strategy adopted involves the additional variable i_{fd} . Hence the optimal current reference generator of Fig. 3 is replaced by three compensators.

VII. RESULTS AND DISCUSSIONS

Fig. 6-Fig. 11 show the system responses to commands following a step increase in local electrical load. Fig. 6,

Fig. 8 and Fig. 10 show responses with optimal currents generated for every torque-speed duo and stored in a lookup table. Fig. 7, Fig. 9 and Fig. 11 show responses with optimal currents generated on-line.

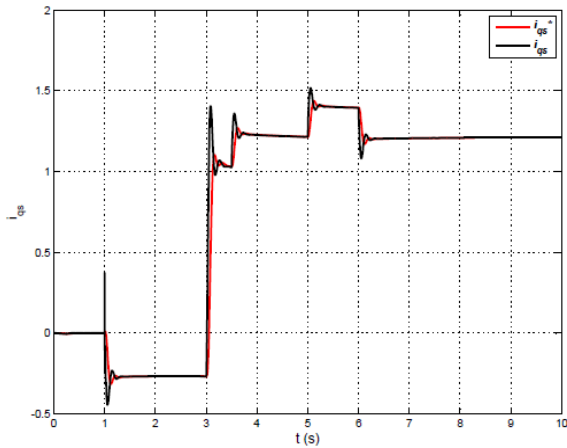


Figure 6. i_{qs}^* reference currents generated off-line.

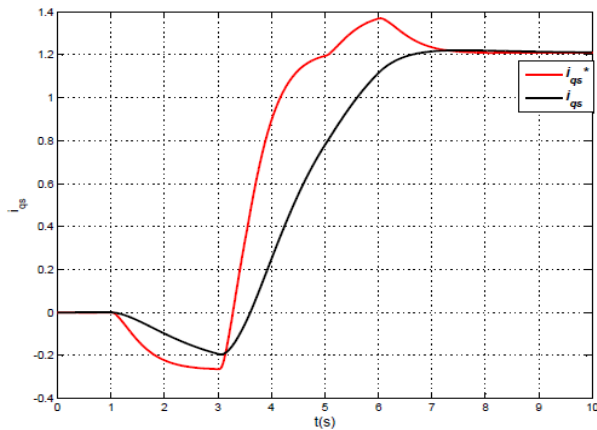


Figure 7. i_{qs}^* reference currents generated on-line.

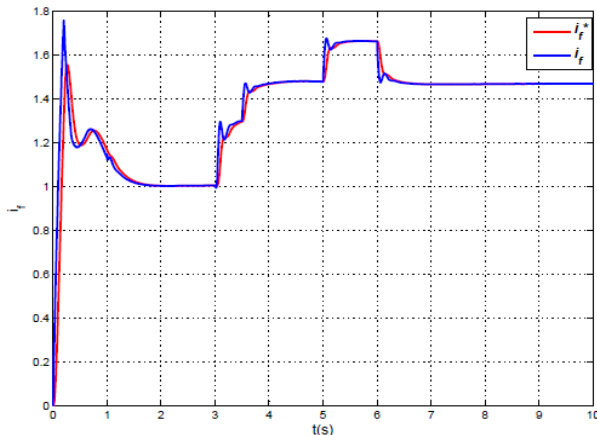


Figure 8. i_f^* reference currents generated off-line.

From the simulation results, it is observed that using pre-calculated torque-speed maps for optimal current generation offers quicker response than generation of the same on-the-fly. However, it is also visible that overshoots and undershoots are prominent.

Storing torque speed related optimal maps may be expensive in terms of random access memory needed but the response is quicker and may be cheaper than on-line

computations in terms of computational processing power. Memory requirements in the stored optimal map strategy can be minimised by restricting the operational range to achieve control objectives.

It is observed that the DC bus voltage fluctuations are less severe with on-line optimal current generation. This is because the time constants of the transients are faster than the computation time of the optimal values. In both methods however, significant stability of the DC bus voltage is observed. This stability is largely due to the combined action of the BESS and DC-DC converter. Incorporating a DC boost converter and BESS may from the controllability perspective, be a cheaper and more stable alternative than having a controlled converter at the terminals of the synchronous machine. This is an area for further analysis.

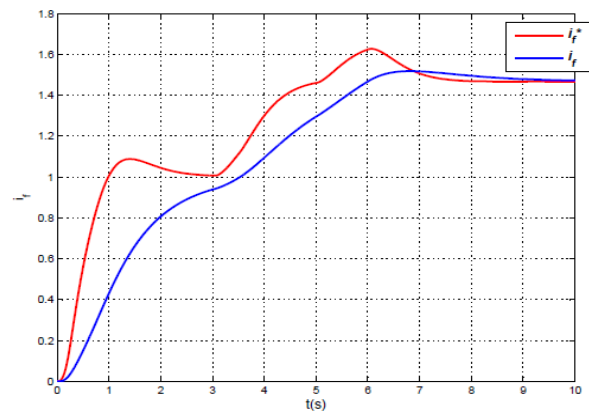


Figure 9. i_f^* reference currents generated on-line.

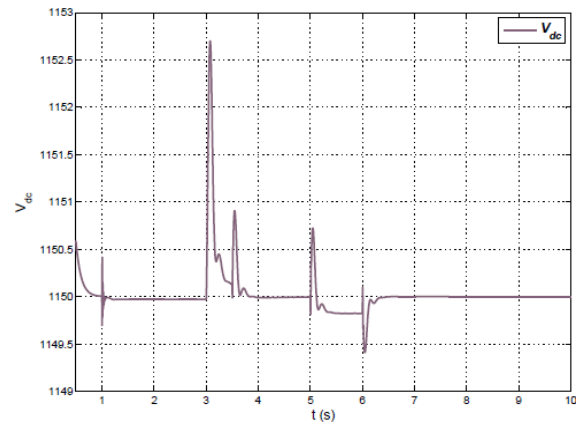


Figure 10. DC bus response with reference currents generated off-line.

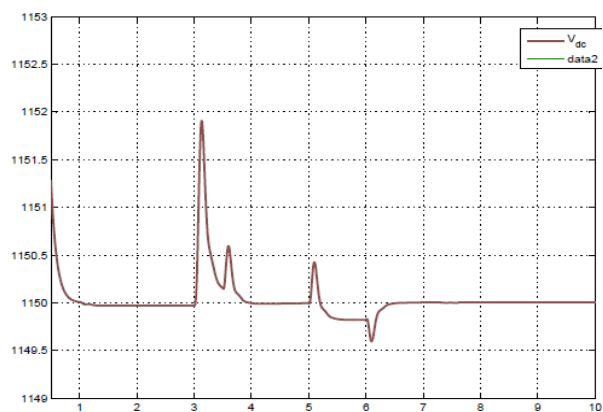


Figure 11. DC bus response with reference currents generated on-line.

VIII. CONCLUSION

This article presented a synchronous generator model suited for optimal control in variable speed, variable output applications within a specified range and compared two methods to generate optimal command currents. An optimal LQR strategy was employed for the generator control and two methods of optimal reference control current generation were compared. It is observed that by pre-defining and bounding a speed range, it is more operationally efficient to calculate and store optimal reference currents off-line than compute them in real time. The advantages of the off-line method are its quick response and reduced computation time.

The efficiency can be improved by more accurate modelling and generation of the torque speed maps. The proposed method can greatly enhance efficiency in control of synchronous generators used in variable speed renewable energy applications.

REFERENCES

- [1] R. Pena, J. Clare, and G. Asher, "Doubly fed induction generator using back-to-back PWM converters and its application to variable-speed wind-energy generation," *IEE Proceedings-Electric Power Applications*, vol. 143, pp. 231-241, 1996.
- [2] A. Petersson, *Analysis, Modeling and Control of Doubly-Fed Induction Generators for Wind Turbines*, Chalmers University of Technology, 2005.
- [3] S. Müller, M. Deicke, and R. W. D. Doncker, "Doubly fed induction generator systems for wind turbines," *IEEE Industry Applications Magazine*, vol. 8, pp. 26-33, 2002.
- [4] R. Datta and V. Ranganathan, "Variable-Speed wind power generation using doubly fed wound rotor induction machine-a comparison with alternative schemes," *IEEE Transactions on Energy Conversion*, vol. 17, pp. 414-421, 2002.
- [5] L. Holdsworth, X. Wu, J. Ekanayake, and N. Jenkins, "Comparison of fixed speed and doubly-fed induction wind turbines during power system disturbances," *IEE Proceedings-Generation, Transmission and Distribution*, vol. 150, pp. 343-352, 2003.
- [6] F. Shibata and K. Taka, "A self-cascaded induction generator combined with a separately controlled inverter and a synchronous condenser," in *Proc. Industry Applications Society Annual Meeting*, 1990, pp. 309-317.
- [7] H. Polinder, F. F. V. D. Pijl, D. Vilder, and P. J. Tavner, "Comparison of direct-drive and geared generator concepts for wind turbines," *IEEE Transactions on Energy Conversion*, vol. 21, pp. 725-733, 2006.
- [8] R. Sharma, T. W. Rasmussen, and B. B. Jensen, "Application of a synchronous generator with a boost converter in wind turbines: An experimental overview," *IET Renewable Power Generation*, vol. 6, pp. 414-423, 2012.
- [9] S. D. Sudhoff and O. Wasynczuk, "Analysis and average-value modeling of line-commutated converter-synchronous machine systems," *IEEE Transactions on Energy Conversion*, vol. 8, pp. 92-99, 1993.
- [10] P. C. Krause, O. Wasynczuk, S. D. Sudhoff, and S. Pekarek, *Analysis of Electric Machinery and Drive Systems*, John Wiley & Sons, 2013.
- [11] P. C. Krause and T. A. Asipo, "Analysis and simplified representations of rectifier-inverter reluctance-synchronous motor drives," *IEEE Transactions on Power Apparatus and Systems*, pp. 962-970, 1969.
- [12] I. Jadric, D. Borojevic, and M. Jadric, "A simplified model of a variable speed synchronous generator loaded with diode rectifier," in *Proc. 28th Annual IEEE Power Electronics Specialists Conference*, 1997, pp. 497-502.
- [13] O. Tremblay, L. A. Dessaint, and A. I. Dekkiche, "A generic battery model for the dynamic simulation of hybrid electric vehicles," in *Proc. IEEE Vehicle Power and Propulsion Conference*, 2007, pp. 284-289.

- [14] B. D. Anderson and J. B. Moore, *Optimal Control: Linear Quadratic Methods*, Courier Corporation, 2007.
- [15] K. Zhou, J. C. Doyle, and K. Glover, *Robust and Optimal Control*, New Jersey: Prentice Hall, 1996.
- [16] C. Jaen, J. Pou, R. Pindado, V. Sala, and J. Zaragoza, "A linear-quadratic regulator with integral action applied to pwm dc-dc converters," in *Proc. 32nd Annual Conference on IEEE Industrial Electronics*, 2006, pp. 2280-2285.
- [17] W. F. Arnold III and A. J. Laub, "Generalized eigenproblem algorithms and software for algebraic Riccati equations," *Proceedings of the IEEE*, vol. 72, pp. 1746-1754, 1984.
- [18] V. Lesic, M. Vasak, G. Stojic, and T. M. Wolbank, "Fault-Tolerant control of wound rotor synchronous generator in wind turbines," in *Proc. International Conference on Electrical Machines*, 2014, pp. 1758-1764.
- [19] M. Haque, L. Zhong, and M. Rahman, "Improved trajectory control for an interior permanent magnet synchronous motor drive with extended operating limit," *Journal of Electrical & Electronics Engineering, Australia*, vol. 22, pp. 49-57, 2003.
- [20] R. Mbayed, G. Salloum, L. Vido, E. Monmasson, and M. Gabsi, "Hybrid excitation synchronous machine control in electric vehicle application with copper losses minimization," in *Proc. 6th IET International Conference on Power Electronics, Machines and Drives*, 2012, pp. 685-690.



James O. Owuor received his B.Sc. degree in electrical engineering in 1996 and MSc degree in electrical power systems and networks in 1998, both from Vinnitsa State Technical University, Ukraine, and his D.Tech. in electrical engineering from Tshwane University of Technology, South Africa in 2014. His research interests are in renewable energy and electrical machines in power systems. He is currently a lecturer in electrical engineering at Masinde Muliro University of Science and Technology, Kenya.



Josiah L. Munda received MSc degree in electrical distribution from Moscow Power Institute and Tver State Technical University, Russia, in 1991, and DEng degree in electrical engineering from the University of the Ryukyus, Japan, in 2002. He is currently an associate professor of electrical engineering at Tshwane University of Technology, South Africa, and is the Director of the Centre for Energy and Electric Power. His research interests are in power system stability, distributed generation systems and microgrids. Prof. Munda is a Registered Engineer in South Africa and Kenya, and is a member of SAIEE and IEEE.



Adisa A. Jimoh received the BEng and the MEng degrees in electrical engineering from Ahmadu Bello University (ABU), Zaria, Nigeria, in 1977 and 1980, respectively, and the Ph.D. degree from McMaster University, Hamilton, ON, Canada, in 1986. He was with ABU until 1992, when he moved to the Research and Development Unit, National Electric Power Authority (NEPA), Lagos, Nigeria. He was with NEPA until 1996 when he moved to the University of Durban-Westville, Durban, South Africa. In 2001, he joined Tshwane University of Technology, Pretoria, South Africa, where is a Professor, the Rand Water Chair in Electrical Engineering and the leader of the Energy and Industrial Power Systems research niche area. His research interests are in electric machines, drives, and power-electronics applications in power systems. Prof. Jimoh is a Registered Engineer in South Africa and is a member of SAIEE and IEEE.